Error Tracking in IKONOS Geometric Processing Using a 3D Parametric Model♥

Thierry Toutin
Natural Resources Canada, Canada Centre for Remote Sensing
588, Booth Street, Ottawa, Ontario, K1A 0Y7

ABSTRACT

Thirteen panchromatic (Pan) and multiband (XS) IKONOS Geo-product images over seven study sites with various environments and terrain were tested using different cartographic data and accuracies with a 3D parametric model developed at the Canada Centre for Remote Sensing, Natural Resources Canada. The objectives of this study were to define the relationship between the final accuracy and the number and accuracy of input data, to track error propagation during the full geometric correction process (bundle adjustment and ortho-rectification), and to advise on the applicability of the model in operational environments.

<p>

When ground control points (GCPs) have an accuracy poorer than 3 m, 20 GCPs over the entire image is a good compromise to obtain a 3- to 4-m accuracy in the bundle adjustment. When GCP accuracy is better than 1 m, 10 GCPs are enough to decrease the bundle adjustment error of either panchromatic or multiband images to 2-3 m. Because GCP residuals reflect the input data errors (map and/or plotting) these errors did not propagate through the 3D parametric model, and the internal accuracy of the geometric model is thus better (around a pixel or less).

<p>

Quantitative and qualitative evaluations of ortho images were thus performed with either independent check points or overlaid digital vector files. Generally, the measured errors confirmed the predicted errors or even were slightly better, and 2-4 m positioning accuracy was achieved for the ortho images depending upon the elevation accuracy (DEM and grid spacing). To achieve a better final positioning accuracy, such as 1 m, a 1-2 m accurate DEM with fine grid spacing is required in addition to well-defined GCPs with an accuracy of 1 m.

INTRODUCTION

The generation of high-resolution imagery using previously proven defence technology provides an interesting source of data for digital topographic mapping as well as

♥ Published in Photogrammetric Engineering & Remote Sensing, 2002, 68(11):9.

thematic applications such as agriculture, forestry, and emergency response (Kaufmann und Sulzer, 1997; Konecny, 2000). Technical informations regarding the new US civilian satellites with their future applicability to Earth sciences have been summarized by Fritz (1996). IKONOS, successfully launched on 24 September 1999, was the first civilian satellite with these new high-resolution sensors: 1-m panchromatic (Pan) and 4-m multiband (XS) images. In addition, the off-nadir viewing capability (up to 60º in any azimuth) is an important characteristic because it improves the revisit rate to between two and three days, and enables the acquisition of in-track stereo-images. Users can then apply traditional 3D photogrammetric techniques with the stereo-images to extract accurate planimetric and elevation information.

To be prepared for the appropriate use of this new source of data, different research studies have addressed the potential of high-resolution imagery for mapping. A research study at the National Mapping Agency of Great Britain used simulated 0.2-m and 1-m Pan images derived from 1:7,500-scale aerial photos and XS 4-m images from the Compact Airborne Spectrographic Images (Ridley *et al.*, 1997). Some results indicated that the future high-resolution satellite imagery would have potential for improving the existing National Topographic Database of Great Britain from 1-m panchromatic images as well as automating the detection of topographic feature change from 4-m XS images. In an other research study, a theoretical analysis based on in-track and across-track stereo-mapping techniques demonstrated that high-resolution satellite imagery could be used for the generation and updating of national mapping products in the United States, but only if photogrammetric processing were employed (Li, 1998). Based on this theoretical analysis, an evaluation of the potential accuracy of ground points was performed using IKONOS stereo-images simulated from aerial photos (Zhou and Li, 2000). Without ground control points (GCPs), a positioning accuracy of 12 m in the three axes (X, Y and Z) was achieved and with 24 GCPs the accuracy was improved to 3 m in planimetry (X and Y) and 2 m in elevation. More recently, preliminary accuracy tests with real images having a viewing angle of 39º and using a 3D parametric geometric correction model were performed with few accurate GCPs (Toutin and Cheng, 2000; Davies and Wang, 2001). The results of the two research studies demonstrated positioning accuracy of 2-3 m and confirmed the high mapping potential of IKONOS images.

This paper expands on the above-mentioned preliminary results related to the geometric processing and ortho-rectification with digital elevation model (DEM) of IKONOS Geo products. A larger data set of IKONOS images (1-m Pan and 4-m XS) were acquired with 10º to 30º viewing angles at different azimuth angles over international study sites (low-to-high relief, urban, semi-urban, semi-rural or rural areas). Different topographic data and accuracy are used to geometrically process the images with a multi-sensor geometric model developed at the Canada Centre for Remote Sensing (CCRS), Natural Resources Canada (Toutin, 1995) and adapted to IKONOS images (Toutin and Cheng, 2000). In addition, this paper tracks error propagation from the input data to the final

ortho image. Different cartographic parameters affecting accuracy, such as the definition, number, location, and accuracy of GCPs as well as the accuracy and grid spacing of the DEM are also evaluated. Finally, possible future research studies and advice for operational uses as a function of these results are presented.

METHOD DESCRIPTION OF IKONOS GEOMETRIC PROCESSING

The 3D CCRS parametric model

The 3D CCRS parametric model was originally developed to suit the geometry of push-broom scanners, such as SPOT-HRV, and have also benefited from theoretical work in celestial mechanics to better determine the satellite's osculatory orbit and parameters (Toutin, 1983). The model was subsequently adapted as an integrated and unified geometric modelling to geometrically process multi-sensor images (Toutin, 1995). The geometric modelling is integrated because in the final equations, which represents the well-known collinearity condition, it takes into account the different distortions relative to the global geometry of viewing, i.e.:

- the distortions relative to the platform (position, velocity, orientation),
- the distortions relative to the sensor (orientation angles, instantaneous field of view, detection signal integration time),
- the distortions relative to the Earth (geoid-ellipsoid including elevation), and
- the deformations relative to the cartographic projection (ellipsoid - cartographic plane).

In summary, the collinearity equations of a ground point are first written in the instrumental reference system and converted into the cartographic projection system using elementary transformations (rotations and translations), which are functions of the parameters describing the distortions previously mentioned (Toutin, 1983). The 3D parametric model integrates the following transformations:

- rotation from the sensor reference to the platform reference;
- translation to the Earth's centre;
- rotation which takes into account the platform time variation;
- rotation to align the z-axis with the image centre (M_0) on the ellipsoid;
- translation to the image centre (M_0);
- rotation to align the y-axis in the meridian plane;
- rotation to have xM_0 y tangent to the ellipsoid;
- rotation to align the x-axis in the image scan direction; and
- rotation-translation into the cartographic projection.

The integration of the different distortions and the derivation of the equations and of the parameters are outside the scope of this paper, but the final results, which link the 3D cartographic coordinates to the image coordinates is given by (Toutin, 1983):

$$Pp + y\,(1 + \delta\gamma X) - \tau H - H_o \Delta T^* = 0 \qquad (1)$$

$$X + \theta\ H/\cos\chi + \alpha q(Q + \theta X - H/\cos\chi) - Q\Delta R = 0 \qquad (2)$$

where $$X = (x - ay)(1 + h/N_o) + by^2 + cxy \qquad (3)$$

and $$H = h - x^2/2N_o \qquad (4)$$

Each parameter is given using a mathematical formula (Toutin, 1983) that represents the physical realities of the full viewing geometry (satellite, sensor, Earth, map projection):

H	is the altitude of the point corrected for Earth curvature;
H_o	is the satellite elevation at the image centre line;
N_o	is the normal to the ellipsoid;
a	is mainly a function of the rotation of the Earth;
α	is the instantaneous field-of-view;
p, q	are the image coordinates;
P, Q	are the scale factors in Y and X, respectively;
τ and θ	are a function of the leveling angles in Y and X, respectively;
ΔT^* and ΔR	are the non-linear variations in attitude if they exist (ΔT^*: combination of pitch and yaw, ΔR: roll);
x, y and h	are the ground coordinates;
b, c, χ, $\delta\gamma$,	are 2nd-order parameters, which are a function of the total geometry, e.g., satellite, image and Earth.

Each of these parameters is in fact the combination of several correlated variables of the viewing geometry, so that the number of unknown parameters has been reduced to an independent decorrelated set. As examples of combinations of several variables, we have:

- the orientation of the image is a combination of the platform heading due to orbital inclination, the yaw of the platform, the convergence of the meridian;
- the scale factor in along-track direction is a combination of the velocity, the altitude and the pitch of the platform, the detection signal time of the sensor, the component of the Earth rotation in the along-track direction; and
- the levelling angle in the across-track direction is a combination of platform roll, the viewing angle, the orientation of the sensor, the Earth curvature; etc.

This 3D parametric model has been applied to visible and infra-red (VIR) data (Landsat

5 & 7, SPOT, IRS, ASTER, and KOMPSAT), as well as radar data (ERS, JERS, SIR-C and RADARSAT) with three to six GCPs. Even though detailed sensor/satellite information for IKONOS is not released by Space Imaging, the model has been adapted by transforming the correlated variables of each parameter by taking into account the image characteristics and the available information in the metadata file (Toutin and Cheng, 2000). This 3D parametric model applied to different image types is robust and not sensitive to GCP distribution as soon as there is no extrapolation in planimetry and elevation (Toutin, 1995). Based on good quality GCPs, the accuracy of this model is within one-third of a pixel for medium-resolution images and one resolution cell for radar images and around one to two pixels for high-resolution images.

The geometric processing steps

Since the geometric processing of IKONOS images is the same than for other images (data collection and pre-processing, bundle adjustment with GCPs and ortho-rectification with DEM), the four key processing steps are only summarized:

1. Acquisition and pre-processing of the remote sensing data (images and metadata) to determine an approximate value for each parameter of the 3D parametric model;

2. Acquisition of cartographic data: collection of GCPs with their 3D cartographic coordinates and 2D image coordinates and of the DEM;

3. Computation of the 3D parametric model, initialized with the approximate parameter values and refined by an iterative least-squares bundle adjustment with the GCPs; and

4. Ortho image generation with a DEM into the user cartographic projection, using the previously-computed model parameters for the geometric aspect and a cubic-convolution resampling kernel for the radiometric aspect.

The research addresses not only the geometric processing but also the error propagation of the input data along the processing steps and the accuracy of the two main processing steps (Steps 3 and 4) either:

A. With independent check points (ICPs) during the computation of the bundle adjustment using different numbers and accuracy of GCPs; or
B. By overlaying or comparing digital vector data or ICPs with the ortho images.

STUDY SITES and DATA SET

Seven international study sites with different environments and relief were used in this

research study (Table 1):

1. Toronto, Ontario, Canada, a sub-urban environment with a flat topography and a 60-m elevation range;
2. Beauport, Quebec, Canada, a residential and semi-rural environment with a hilly topography and a 500-m elevation range;
3. Toulouse, France, an sub-urban environment with a flat topography and a 100-m elevation range;
4. Trier, Germany, an urban and semi-rural environment with a rolling topography and a 300-m elevation range;
5. Dresden, Germany, a rural environment with a rolling topography and a 300-m elevation range (Meinel *et al.*, 2001);
6. Caracas, Venezuela, a urban and rural environment with a mountainous topography and a 2200-m elevation range (Arismendi *et al.*, 2000); and
7. Luzern, Switzerland, an urban and rural environment with a mountainous topography and a 2000-m elevation range.

Table 1: Study site descriptions with environment, relief and elevation variation (ΔZ); IKONOS images with mode, collection (Coll.) and azimuth angles; and cartographic data with number of GCPs, and accuracy of the planimetry (Plani.) and the DEM. For the Dresden study site, two sets of GCPs were collected with different cartographic accuracies.

Study Site	Environment Type	Relief ΔZ	IKONOS Image			Cartographic Data		
			Mode	Coll.	Azimuth	GCPs	Plani.	DEM
Toronto Canada	Sub-urban	Flat 60 m	Pan	51º	21º	30	0.5 m	5 m
Beauport Canada	Residential Semi-rural	Hilly 500 m	Pan Pan	63º 63º	322º 252º	55	3-7 m	5 m
Toulouse France	Sub-urban Rural	Flat 100 m	Pan XS	70º	138º	33	1 m	5 m
Trier Germany	Urban Semi-rural	Rolling 300 m	XS	65º	177º	23	0.5 m	5 m
Dresden Germany	Rural	Rolling 300 m	Pan XS	71º	335º	112 118	1) 4 m 2) 1 m	1 m
Caracas Venezuela	Urban Rural	Steep 2200 m	Four Pan	59º 65º 73º 76º	12º 46° 71° 122º	30	5 m	5 m
Luzern Switzerland	Urban Rural	Steep 1800 m	Pan	68º	256º	35	5 m	

For each site, IKONOS Geo-product data, as provided by Space Imaging, covering an area of approximately 10 km by 10 km, were acquired either in Pan mode (1-m pixel spacing) and/or in XS mode (4-m pixel spacing). International collaborators acquired cartographic data for some of the sites. Table 1 gives specific collection and azimuth

angles, number of GCPs as well as planimetric and DEM accuracy for each site.

1. For Toronto, Ontario, Canada, a Pan image was acquired on 23 April 2000. Map coordinates were obtained from 20-cm pixel orthophotos and a 2-m grid spacing DEM;
2. For Beauport, Quebec, Canada, two Pan images were acquired on 03 January 2001. Map coordinates were obtained from six 1-m pixel orthophotos and a 5-m grid spacing DEM. However, a mean positioning error of 5 to 7 m in the X direction was found between the different orthophotos; this error is mainly due to a 5-m DEM error during the orthophoto generation;
3. Toulouse, France, Pan and XS images were simultaneously acquired on 14 May 2000. Map coordinates were obtained from a 0.5-m pixel orthophoto mosaic and a 10-m grid spacing;
4. Trier, Germany, a XS image was acquired on 13 June 2000. Map coordinates were obtained using differential GPS and a 20-m grid spacing DEM;
5. Dresden, Germany, Pan and XS co-registred images were simultaneously acquired on 01 August 2000. Map coordinates were obtained from 1:10,000-scale topographic maps and a 1-m grid spacing laserscanning DEM. In addition, a second set of map coordinates (118 GCPs) were obtained from 0.4-m pixel orthophoto mosaic with a 1-m accuracy;
6. Caracas, Venezuela, four Pan in-track images were acquired form the same orbit on 30 December 1999. Map coordinates were obtained from 2.5-m pixel orthophotos and a 5-m grid spacing DEM; and
7. Luzern, Switzerland, a Pan image was acquired on 22 April 2000. Map coordinates were obtained from 1.25-m pixel images of scanned 1:25,000-scale topographic maps.

Because processing is performed on the entire image area, GCPs cover the total surface (100 km^2) with points at the lowest and highest elevation to avoid extrapolations, both in planimetry and elevation. In general, the plotting accuracy for Pan images is about 1 to 2 pixels in urban and suburban areas and 2 to 3 pixels in rural and mountainous areas due to the difficulty finding and locating ground features accurate to 1 m. For XS images, the plotting accuracy depends upon the collection method used to evaluate different possibilities and the type of environment:

- in the Trier site (Site 4), GCPs were directly plotted on the XS image, mostly in the urban environment with an accuracy of one-half pixel (about 2 m);
- in the Dresden rural site (Site 5), GCPs were imported from Pan image with the same 2- to 3-m accuracy, but their coordinates were computed by dividing the Pan image coordinates by four; and
- in the Toulouse sub-urban site (Site 3), GCPs collected on the Pan image were re-plotted on the XS image with an accuracy better than one pixel. However, these points were not necessarily the best-defined points in the XS image.

RESULTS AND DISCUSSIONS

Error propagation can be tracked along the geometric processing steps with bundle adjustment results as a function of GCP numbers, location, and accuracies as well as with the ortho images as a function of DEM accuracy and spacing. It should be noted that the processing was performed on the full image size (about 100 km^2), and not just on small sub-area.

Bundle Adjustment Results

The first test performed used all the GCPs of each image in the bundle adjustment. Table 2 summarizes these results with the residuals for the GCPs (root mean square (RMS) and minimum/maximum). With the 3D parametric model, the residuals do not reflect the modelling accuracy but rather the error of the input data when there are more GCPs than the minimum required (Toutin, 1995). In fact, Table 2 shows that the RMS residuals are generally in the same order of magnitude as the GCP planimetric accuracy (plotting and map), in addition to the propagation of GCP Z-error, depending on the view and the azimuth angles.

Table 2: Bundle adjustment results for the study sites with the number and accuracy (in planimetry and elevation) of GCPs, and the root mean square (RMS) and Min./Max. residuals (in meters) for the GCPs. For the Dresden study site, there are two sets of results as a function of different GCP numbers and accuracies. For the Beauport and Caracas study sites, the results are given for the different panchromatic images (A, B, C, D).

Study Site	GCP Number	GCP Accuracy	RMS Residuals		Min./Max. Residuals	
			X	Y	X	Y
Toronto	30	0.5 m, 1 m	0.8	1.1	-1/2	-3/2
Beauport_A	56	3-7 m, 5 m	5.8	2.2	-10/11	-5/5
Beauport_B	56	3-7 m, 5 m	6.0	2.1	-11/12	-5/5
Toulouse_Pan	33	1 m, 5 m	2.9	1.7	-5/7	-3/4
Toulouse_XS	33	1 m, 5 m	3.3	2.5	-7/7	-5/4
Trier	22	0.5 m, 5 m	1.4	1.4	-3/4	-2/3
Dresden_Pan1	112	4 m, 1 m	5.1	5.6	-13/12	-18/17
Dresden_XS1	112	4 m, 1 m	5.1	5.6	-13/12	-18/17
Dresden_Pan2	118	1 m, 1 m	2.3	1.6	-5/6	-4/5
Dresden_XS2	118	1 m, 1 m	2.3	1.6	-5/6	-4/5
Caracas_A	27	5 m, 5 m	2.7	3.4	-6/4	-6/7
Caracas_B	35	5 m, 5 m	5.3	5.3	-11/12	-9/14
Caracas_C	38	5 m, 5 m	5.1	2.2	-13/8	-4/4
Caracas_D	24	5 m, 5 m	2.8	4.1	-5/5	-9/7
Luzern	76	5 m, 5 m	5.6	2.8	-12/11	-8/5

With the Beauport site (Site 2), the GCP RMS residual is larger in *X* (5.8 m) than in *Y* (2.2 m), reflecting the larger map *X*-error (5 to 7 m) than the *Y*-error (3 m). Due to the GCP collection in the XS image of the Toulouse site (Site 3), the residuals relative to pixel spacing are slightly worse with the Pan image than with the XS image. With the Dresden site (Site 5), the residuals are better with the accurate GCP coordinates data set (Pan2 versus Pan1; XS2 versus XS1). With mountainous Luzern site (Site 7), the propagation of GCP *Z*-error (around 2 to 3 m) is principally included in the *X* direction (collection and azimuth angles of 68º and 256º, respectively), which explains the larger RMS residual in *X*.

Refining this first analysis demonstrates that the RMS residuals are slightly larger than the GCP planimetric accuracy when the input coordinates had an accuracy of 1-m or worse (for example, Toronto, Toulouse, Trier and Dresden_2). The reverse occurred when the input coordinates had an accuracy of 5 m (for example, Beauport, Dresden_1, Caracas and Luzern). In fact, plotting error is the major source of error in the first scenario mentioned above (2 to 3 m versus 1 m) while map coordinate error is the major source in the second scenario (5 m versus 2 to 3 m). When the plotting error is the major source of error, the explanations are:

- the RMS residual differences between Pan and XS images (Toulouse) are not proportional to pixel spacing since the plotting accuracy is about the same (2-3 m);
- the RMS residuals in urban environments (Toronto, Trier) are better than the RMS residuals in rural environments (Toulouse, Dresden_2) because GCP definition and plotting are more accurate in urban environments; and
- the RMS residuals for XS images are correlated with the plotting error: e.g., the best results for Trier (RMS and plotting error of 1.4 m and 2 m, respectively) and the worse results for Toulouse (RMS and plotting error of 3 m and 4 m, respectively). In the Toulouse site the GCPs collected and exported from the Pan image were not necessarily the best-defined points in the XS image.

The analysis of the *X*-*Y* minimum/maximum residuals, which are generally around twice or sometimes three times the RMS residuals, demonstrates that the 3D parametric model is stable over the entire images without generating local errors. The use of overabundant GCPs (six is the theoretical minimum) in the least-squares bundle adjustment reduced the propagation of different input data errors (plotting and/or cartographic) in the 3D parametric model, but conversely these input errors are reflected in the residuals.

However, unbiased validation of the positioning accuracy has to be realized with ICPs, which were not used in the 3D parametric model calculation. Different GCP/ICP configurations using the data from the Dresden site, which had the most complete data set, were evaluated to find the optimal number of GCPs in relation to the error of the cartographic coordinates. With the Dresden_Pan1 data set, the number of 4-m accurate

GCPs varied from 112 to 6, and the bundle adjustment results (Figure 1) were evaluated on the 118 1-m accurate ICPs from the second set of coordinates. With the Dresden_Pan2 data set, the number of 1-m accurate GCPs varied from 70 to 6 and the bundle adjustment results (Figure 2) were evaluated on the remaining 48 to 112 ICPs, respectively, of this data set.

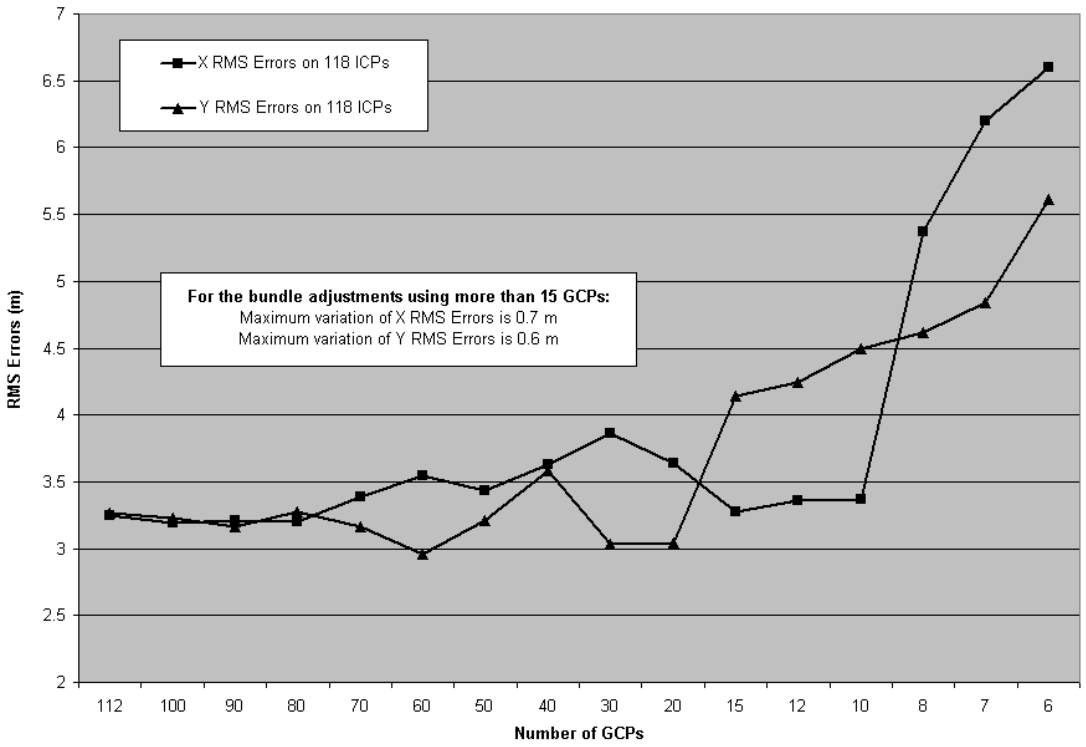

Figure 1. Root mean square (RMS) errors (in meters) on 118 1-m accurate ICPs from the least-squares bundle adjustment computed with GCPs varying from 112 to 6 for the Dresden study site. The variation of RMS errors for the bundle adjustment using more than 15 GCPs is not significant.

In Figure 1, the RMS errors on ICPs were always higher than 3 m regardless of the number of GCPs (even with a large redundancy of GCPs). The variations (less than 0.7 m) of RMS errors between the different bundle adjustments using 112 to 15 GCPs were not significant. Below 10-12 GCPs, the input errors (mainly the cartographic error) propagated more into the 3D parametric model due a small degree of freedom in the least-squares adjustment. Consequently, 15 to 20 GCPs were a good compromise to maintain a 3 m accuracy, which reflects the cartographic error (4 m). On the other hand when using the 1-m accurate GCP coordinates (Dresden_Pan2) (Figure 2), the RMS errors on ICPs were consistently below 2 to 3 m with slightly better results in the *Y*-coordinate regardless of the number of GCPs. The variations (less than 0.3 m) of RMS errors between the different bundle adjustments using 70 to 9 GCPs were not

significant. Below 9 GCPs, the input errors (mainly the plotting error) propagated more into the model due a small degree of freedom in the least-squares bundle adjustment. Ten 1-m accurate GCPs were then a good compromise to maintain a 2 m accuracy, which reflects the plotting error (2 to 3 m).

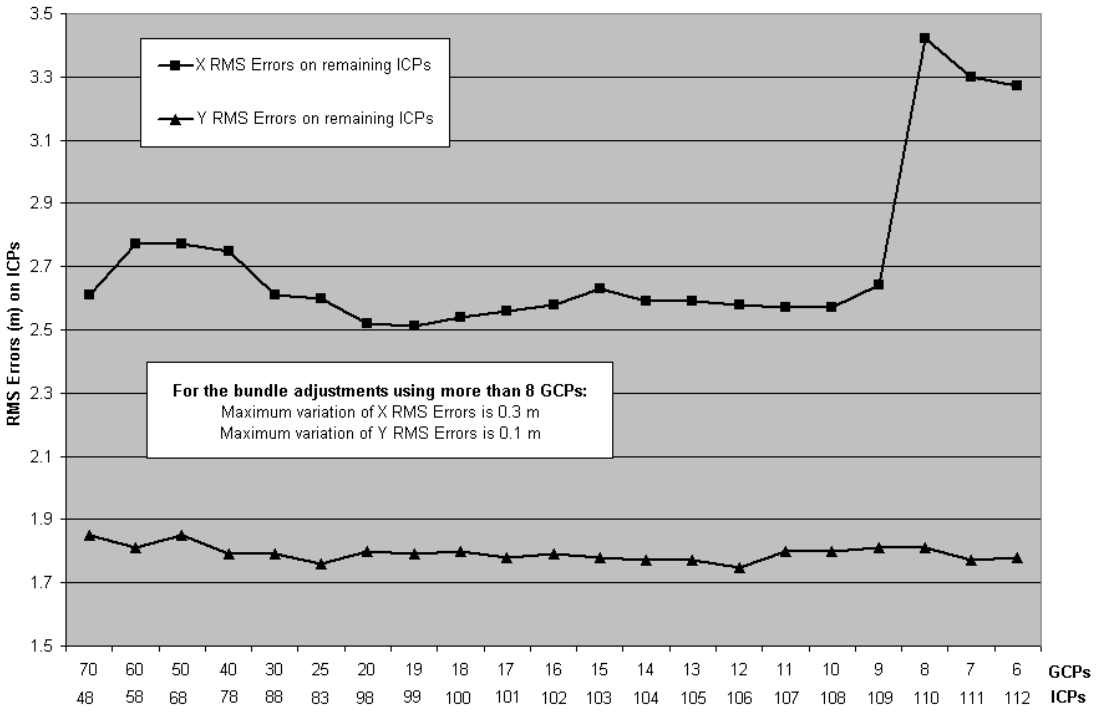

Figure 2. Root mean square (RMS) errors (in metres) on 1-m accurate ICPs from the least-squares bundle adjustment computed with GCPs varying from 70 to 6 for the Dresden study site. The variation of RMS errors for the bundle adjustment using more than 9 GCPs is not significant.

These results on the number of GCPs as a function of their cartographic accuracy (20 GCPs for 5-m accurate coordinates and 10 GCPs for 1-m accurate coordinates) were applied on all data sets. Table 3 shows the statistical results of the bundle adjustment with the number of GCPs/ICPs and the RMS and minimum/maximum errors on the ICPs. For some of the data sets (such as Toronto and Caracas), a smaller number of GCPs were used to keep enough ICPs for the statistical evaluation. When the cartographic coordinates had an accuracy of 1 m (such as for Toronto, Toulouse, Trier and Dresden_2), RMS errors were always around 2 to 3 m; however, slightly worse results occurred for Toulouse. Consequently, the RMS errors reflect the different GCP plotting error on each image depending upon the environment. When the cartographic coordinates had an accuracy of 5 m (such as for Beauport, Dresden_1, Caracas and Luzern), the RMS errors were a little worse than 3 to 5 m. However, slightly worse

results occurred for Beauport in the *X* direction due to the orthophoto *X* error, as well as for Caracas due to the reduced number of GCPs: 12 instead of 20 reduced the advantages of least-squares adjustment. Consequently, the RMS errors reflect the cartographic coordinate errors of each study site. Finally, the RMS errors on ICPs were about the same (10 to 15 percent higher) as the RMS residuals on GCPs (Tables 3) and were in the same order of magnitude as the input data errors. RMS residuals on GCPs can thus be used as the *a priori* mapping error in operational environments, when taking into account the cartographic data errors. Most of the comments and explanations given for Table 2 results then applied to Table 3 results: i.e., the results of the bundle adjustment reflect the cartographic or plotting errors, which do not propagate through the 3D parametric model, but rather through the residuals/errors. In fact, the model filtered random or systematic errors.

Table 3: Bundle adjustment results for all study sites with the number of GCPs and ICPs, and the root mean square (RMS) and Min./Max errors (in meters) for the ICPs. For the Dresden study site, there are two sets of results as a function of different GCP numbers and accuracies. For Beauport and Caracas study sites, results are given for the different Pan images (A, B, C, D).

Study Site	GCP Number	ICP Number	RMS Errors		Min./Max. Errors	
			X	Y	X	Y
Toronto	7	23	1.3	1.3	-3/3	-3/2
Beauport_A	20	36	7.5	2.7	-16/6	-2/6
Beauport_B	20	36	7.6	2.6	-16/11	-4/7
Toulouse_Pan	10	23	3.9	1.8	-8/3	-3/5
Toulouse_XS	10	23	4.9	3.3	-5/11	-6/5
Trier	10	12	2.3	1.8	-3/5	-2/4
Dresden_Pan1	20	118	4.1	2.7	-8/4	-5/8
Dresden_XS1	20	118	4.1	2.7	-8/4	-5/8
Dresden_Pan2	10	108	2.9	1.7	-7/7	-4/5
Dresden_XS2	10	108	2.9	1.7	-7/7	-4/5
Caracas_A	12	15	2.9	3.9	-6/4	-6/7
Caracas_B	12	23	6.4	4.4	-11/12	-9/14
Caracas_C	12	26	6.9	4.4	-13/8	-4/4
Caracas_D	12	12	3.4	4.4	-5/5	-9/7
Luzern	20	56	5.8	3.0	-10/11	-8/9

The last test performed on bundle adjustment was related to various distributions of GCPs. The results with different study sites demonstrated that the 3D parametric model was not sensitive to GCP distribution in accordance with previous results (Toutin, 1995). It is well known that extrapolation in planimetry outside of the GCP boundary is not recommended. However, it is not well recognized that large extrapolation should also not be applied in the elevation direction. To test the impact of elevation extrapolation, data from the Caracas

and Luzern study sites were used because they have more than 2000-m elevation difference. When the highest GCP used in the bundle adjustment was 1000 m lower than the mountain summit (generating a 1000-m extrapolation) the largest planimetric errors on the highest ICPs were around 20 to 30 m. This error was reduced to 10 m when the elevation extrapolation was reduced to 500 m.

Ortho Image Results

Ortho images werew generated in the conformal cartographic projection system of the user for four different data sets (Beauport_A, Trier, Dresden and Caracas). These sites were chosen because digital vector files with 1- to 3-m accuracy, depending of the study site, were available. The ortho-correction process uses the parameters of the geometric model previously determined in the least-squares bundle adjustment. Because the geometric model takes into account the elevation distortion, elevation information is needed to create accurate ortho images. Elevations generally extracted from DEM have errors, which propagate through the rectification process in addition to the previous errors of the bundle adjustment process. The elevation errors for the data sets are mainly dominated by two sources: the error on the elevation at the DEM grid point and the error due to the linear interpolation between grid points, which depends of the terrain slopes. For Trier, a 20-m grid spacing DEM with a 5-m accuracy and a rolling relief with slopes less than 10º generate an elevation error of about 5 m (no interpolation error). On the other hand, for Caracas, a 5-m grid spacing DEM with a 5-m accuracy and a mountainous relief with slopes less than 45º generate an elevation error of about 6 m.

To compute the propagation of elevation errors into the ortho image as a function of the viewing angle, curves (Figure 3), mathematically computed with the elevation parameters of the geometric model, were used (Toutin, 1995). These curves give the relationship between the acquisition viewing angle of the image, the elevation error (DEM and interpolation) and the positioning error generated on the ortho image: the knowledge of two parameters enabled the third parameter to be evaluated to better manage the data collection. For example, if a final 1-m positioning accuracy for the ortho image is required while the IKONOS image was acquired with a 30º-viewing angle, which is normally provided by Space Imaging, the elevation used in the ortho-rectification should have a maximum error of 2 m (Figure 3).

On the other hand, for Trier and Caracas_A images acquired with viewing angles of 25º and 31º, the previously computed 5-m and 6-m elevation errors generate positioning errors on the ortho images of about 2 m and 4 m, respectively. Finally, the predicted final circular error of the ortho images, as a combination of the bundle adjustment errors (Table 3) and the elevation error propagation in the ortho-rectification, should be about 4 m and 6 m for Trier and Caracas_A, respectively.

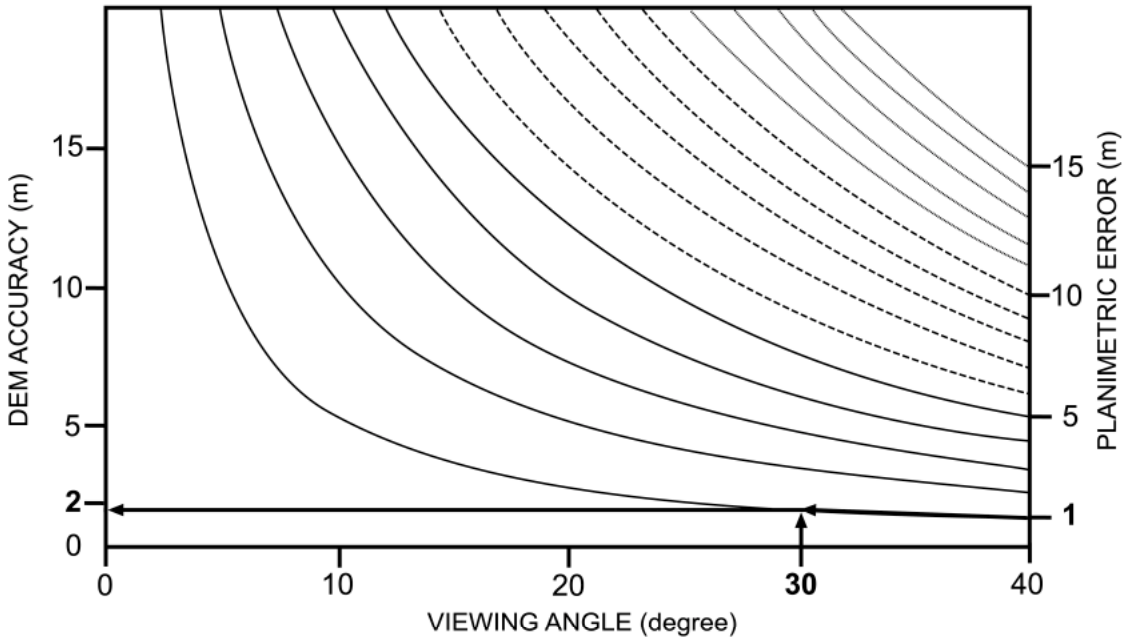

Figure 3. Relationship between the acquisition viewing angle of the image, the elevation error (DEM and interpolation), with the resulting positioning error generated in the ortho image (Toutin, 1995). These curves were computed with the elevation parameter of the 3D parametric model. As example, if a 1-m positioning accuracy for the ortho image is required while the IKONOS image was acquired with a 30º viewing angle (as normally provided by Space Imaging), the elevation used in the ortho-rectification should have an maximum error of 2 m.

To confirm these predicted evaluations, a qualitative and visual evaluation of the ortho images for the four study sites was performed. For the Beauport_A image, a quantitative comparison of the panchromatic ortho image (1-m pixel) was performed with 31 ICPs extracted from 3-m accurate vector lines. RMS errors of 5 m and 3 m with 1.5-m and –0.5-m bias for *X* and *Y* respectively, were computed with no errors larger than 10 m when compared to the vector lines. By performing a qualitative analysis in addition to the quantitative comparison, the vector lines are overlaid on the ortho image (Figure 4, top) and the orthophoto (Figure 4, bottom). The road vector lines are always inside the roads visible in the IKONOS images. By considering the main roads to be 10-m wide a 4-m error could be estimated. These two estimated errors from ICPs (3 m) and vector lines (4 m) are better than a circular error of 8 m directly computed from the ICP errors in the bundle adjustment (Table 3). The 5-m elevation error generated in the ortho-rectification only a 2.5-m error, which is negligible in the error budget. However, the 8-m circular error is biased because the 5- to 7-m *X* error of the orthophotos was included. Finally, when comparing the vector lines of the same roads overlaid on the 1-m orthophoto, the same deviations could be noticed. Hence, this could mean that part of errors came from the 3-m error vector lines. Evaluation of other features, such as secondary roads, rivers and even private

houses confirmed the 4-m error.

Figure 4. Sub-area of the Beauport_A ortho image (1-m pixel spacing, 512 pixels by 512 lines) at the top, and of the Beauport orthophoto (1-m pixel spacing, 512 pixels by 512 lines) at the bottom, with 1:25,000-scale 3-m accurate vector lines overlaid. IKONOS Images © Space Images LLC, 2000.

For the Dresden site, the quantitative comparison of the Pan ortho image (1-m pixel) was independently performed at Dresden, Germany using 31 ICPs extracted from the 0.4-m pixel orthophoto mosaic with 1-m accuracy. RMS errors of 2 m with a 0.5-m bias in both axes were computed with no errors larger than 5 m. The errors were consistent with a circular error of 3 m directly computed from the ICP errors in the

bundle adjustment (Table 3) because the 1-m elevation error has a minor impact in the ortho-rectification process and in the error budget.

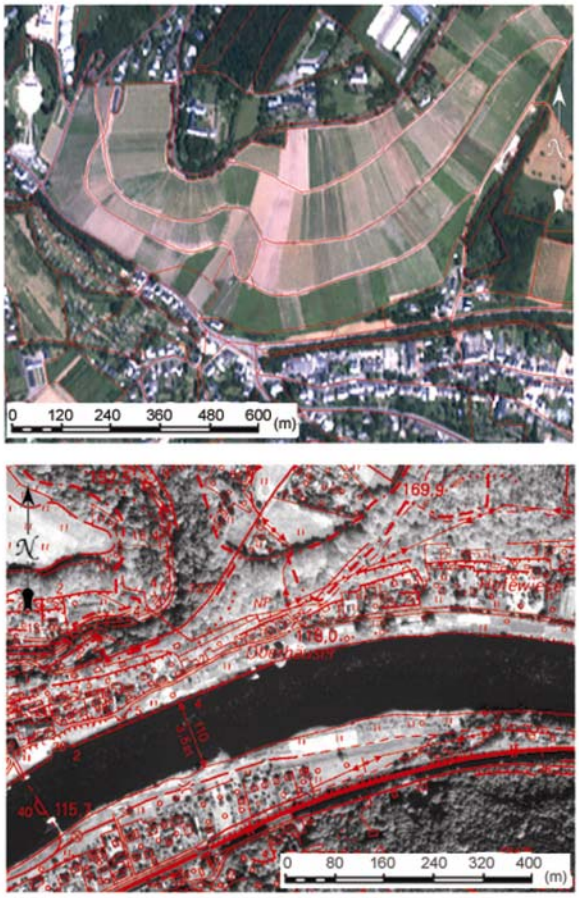

Figure 5. Sub-area of the Trier ortho image (2-m pixel spacing, 640 pixels by 440 lines) at the top, and of the Dresden ortho image (1-m pixel spacing, 940 pixels by 660 lines) at the bottom, with 2-m accurate vector lines overlaid. IKONOS Images © Space Images LLC, 1999, 2000.

Figure 5 shows sub-areas of the XS (2-m pixel) ortho image of Trier (top) and the Pan (1-m pixel) ortho image of Dresden (bottom) with overlaid 2-m accurate vector files from German Topographic Database. Both images with their corresponding vector files were evaluated in Canada and Germany. There is a good superposition between the vectors on the appropriate image features. The Trier sub-area (640 pixels by 440 lines) is the most pronounced relief area, having a 150-m elevation variation along a steep vineyard. The cartographic lines along the slope, such as in the villages appear to exactly conform to the geometry of the ortho image with one-pixel error (2 m). The good superposition is more evident in 3-m wide vineyard tracks. This approximate error evaluation is consistent with and even better than the previously predicted error of 4 m. For the Dresden sub-area (940 pixels by 660 lines), the banks of the river show

positioning errors of no larger than 2 to 3 pixels (2 to 3 m). Other well-defined features, such as roads or city streets visually show the same accurate superposition within the ortho image in accordance with the previously computed ICP accuracy.

Because the four Caracas images were available with some overlaps, a 1-m pixel ortho mosaic was realized. Relative and absolute evaluations were then performed on two areas of the ortho-mosaic. These evaluations occurred in an overlap area of Caracas_A and B images in the mountains (Figure 6), and in a coastal area with overlaid 1:1,000-scale 2-m accurate vector lines (Figure 7).

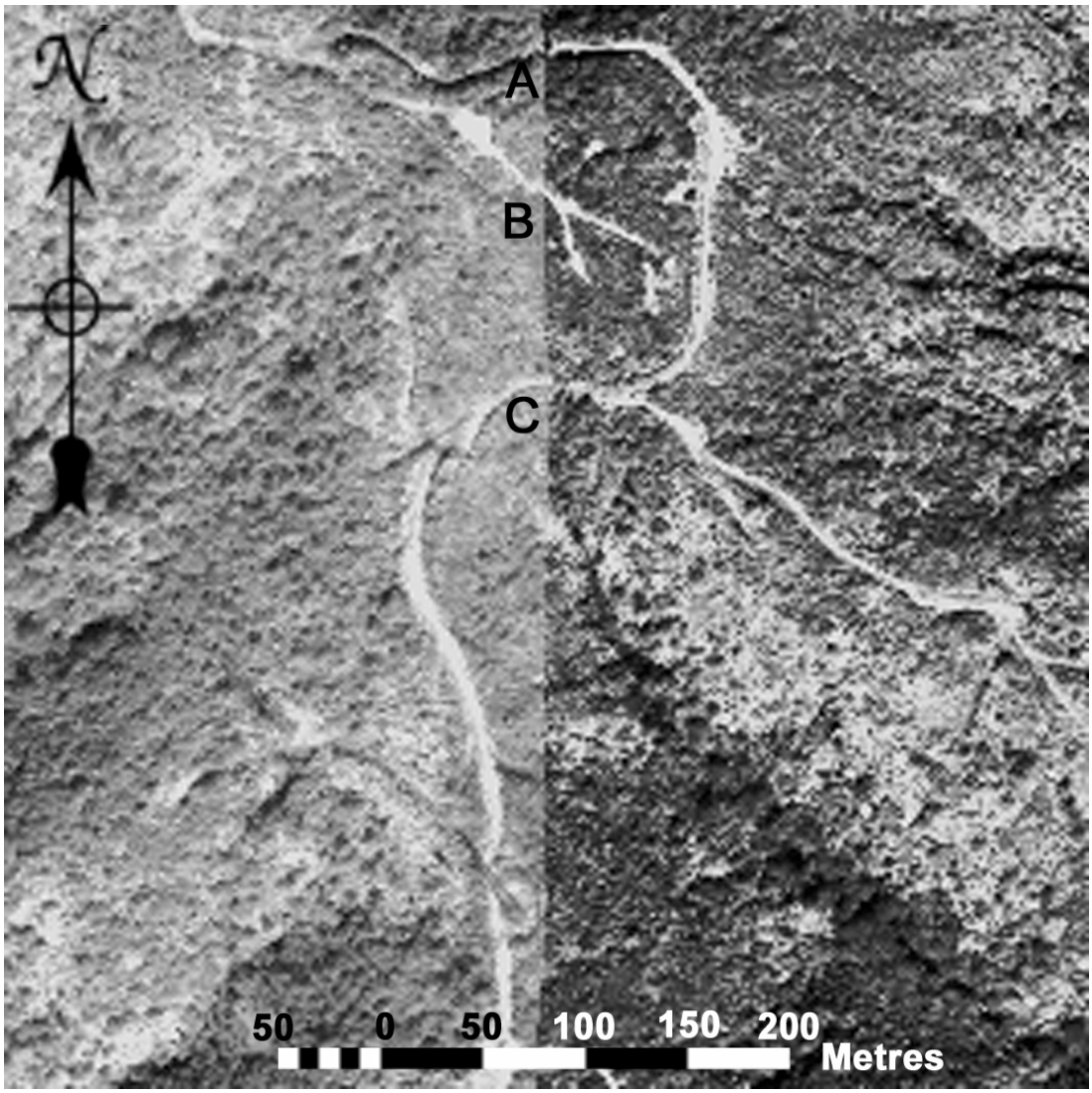

Figure 6. Sub-area (1-m pixel spacing, 512 pixel by 512 lines) of the Caracas_A and _B ortho mosaic at the image overlap area in the mountains. Radiometric variations between the images were enhanced to show the seed. A, B and C are the roads where relative accuracy is evaluated. IKONOS Images © Space Images LLC, 1999.

The radiometric variations between the two images of Figure 6 were increased to show the seed of the mosaic. Thus, the relative accuracy between the images can be evaluated on three mountain roads (A, B and C) to be in the order of 2 m with a maximum error of 6 m for the lowest road (C). The 1:1,000-scale vector lines displayed in Figure 7 show many details not visible on the IKONOS ortho image for defining a precise superposition error. However, using the vectors representing the edge of the 5-m wide largest roads, an absolute accuracy can be approximated to be 3 to 4 m with a maximum error of less than 10 m. This superposition error, more obvious with the sport field on the left side, confirmed the predicted evaluation of 6 m.

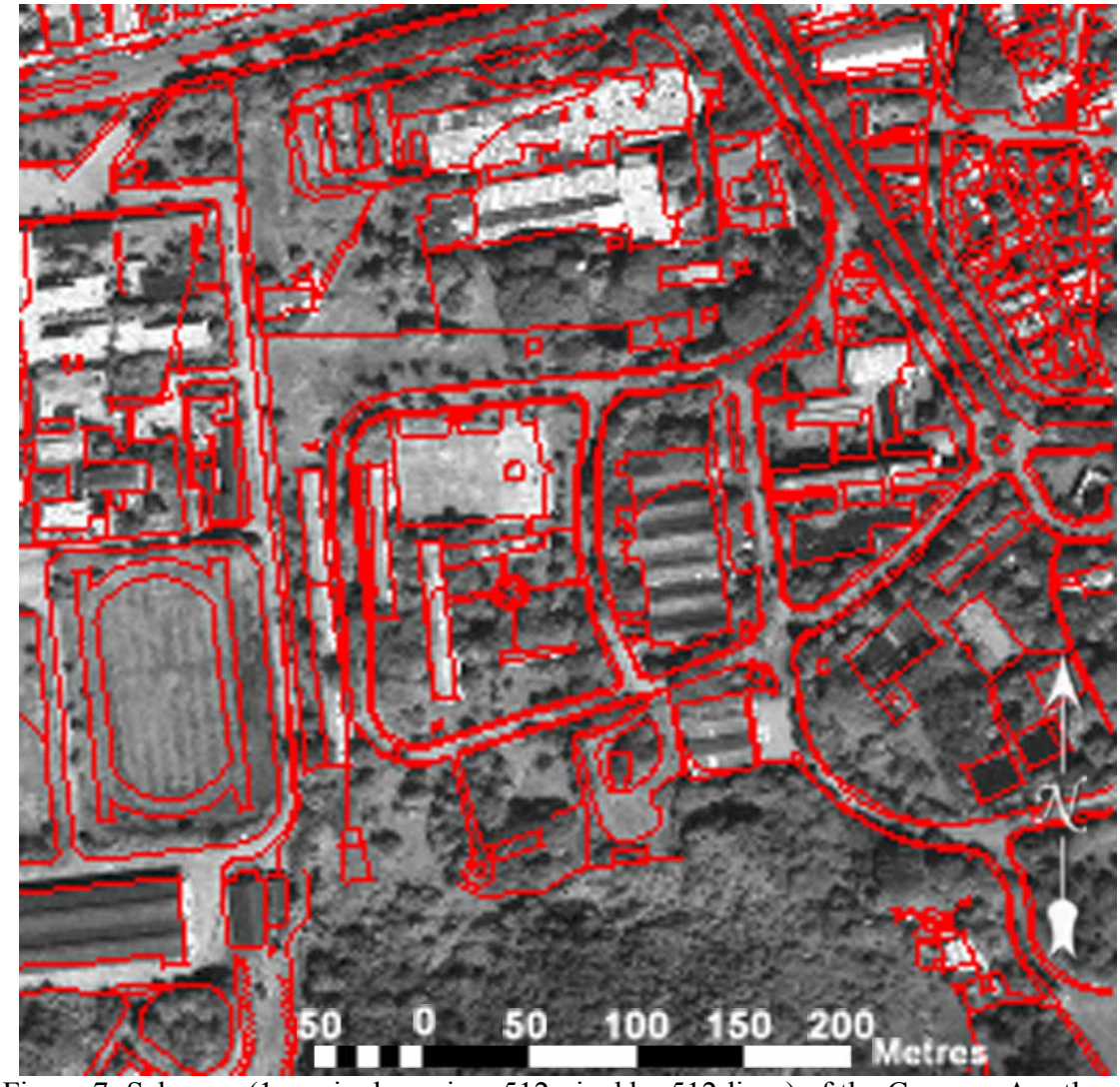

Figure 7. Sub-area (1-m pixel spacing, 512 pixel by 512 lines) of the Caracas_A ortho image at the coastal area with the 1:1,000-scale 1-m accurate vector lines overlaid. IKONOS Images © Space Images LLC, 1999.

CONCLUSION

Thirteen (13) Pan and XS images, acquired by international collaborators over seven study sites with various environments and terrain relief, were tested to evaluate the accuracy of the 3D parametric model developed at CCRS for IKONOS Geo-product images. Cartographic data (digital maps, orthophotos, GCPs, DEM, digital vector files) were acquired from different sources and accuracy. The paper evaluated the potential, the accuracy and the robustness of the 3D parametric model under different aspects. The type of images (Pan or XS); the method of GCP collection; the distribution, number and accuracy of GCPs; and the characteristics of DEM (elevation and grid sampling) versus the terrain relief were addressed with regard to the final accuracy. The error propagation was then tracked during the full geometric correction process (bundle adjustment and ortho-rectification) to advise on the applicability of the model in operational environments.

From the bundle adjustment general results it can be concluded that 20 3-m accurate GCPs are a good compromise to achieve 3- to 4-m error in the bundle adjustment, while 10 1-m accurate GCPs are thus enough to achieve 2- to 3-m accuracy. In the first scenario, the cartographic coordinate error (3 to 5 m) is the major source of error while it is the GCP definition and plotting error (2 to 3 pixels) in the second scenario. Because GCP residuals reflect the input data error, it is thus normal and "safe" to obtain residuals on the same order of magnitude as the GCP error. However, the geometric model will be more accurate because the input error did not propagate into the 3D parametric model. As a matter of fact, a better accuracy of 1-2-m was achieved in the bundle adjustment of Pan and XS images of the Toronto and Trier study sites using accurate GCPs (1- to 2-pixel plotting accuracy **and** a 1-m cartographic accuracy). Because the physical definition and the plotting of GCPs become a key point to obtain sub-pixel accuracy with IKONOS images, future research studies at CCRS will address this key point with signalised targets on the ground for accurate GCP definition.

To track the error during the ortho-rectification, the elevation errors were evaluated as a function of DEM accuracy and grid spacing and of the terrain relief with their impact on the ortho image as a function of the viewing angle. By combining these errors with the bundle adjustment errors, a predicted error for different study sites was then computed. The users can then better "manage" each error in the error budget. Finally, the relative and absolute errors in the different ortho images were measured by comparison with either ICPs extracted from vector lines or overlaid digital vector files. A 2-m accuracy was achieved for some ortho images when the input cartographic data were of good quality and a 4-m accuracy was achieved for the others. Generally, these measured errors confirmed the predicted errors or were even slightly better. To achieve a sub-pixel accuracy, a 1- to 2-m accurate DEM with fine grid spacing is required in addition to the precise GCPs (definition, plotting and cartographic coordinates).

Acknowledgements

The author thanks his international collaborators for the IKONOS and/or cartographic data for the different study sites: Dr. Philip Cheng of PCI Geomatics, Canada for Toronto; Mr. Réjean Matte of Ministère des Ressources naturelles du Québec, Canada for Beauport; Mr. Didier Giacobbo of GDTA, France for Toulouse; Prof. Joachim Hill of Trier University, Germany, for Trier; Dr. Gotthard Meinel of Institut für ökologische Raumentwicklung, Germany for Dresden; Lic. Ramiro Salcedo of the Instituto de Ingenieria, Venezula for Caracas and Mr. Jean-Pierre Perret of the Federal Office of Topography, Switzerland for Luzern. He also thanks MM. René Chénier and Yves Carbonneau of Consultants TGIS inc., Canada for processing the data and the software.

References

Arismendi, J., R. Salcedo, y D. Varela, 2000. Geomorfologia Actual y Cobertura Natural de la Vertiente Norte de la Cordillera de la Costa Afectada por el Evento Hidrometeorologico de Diciembre 99, A Partir de la Interpretacion de Imagenes de Satelite, *Proceedings of IX International Symposium of the LatinAmerican Society of Remote Sensing (SELPER),* 6-10 November, Puerto Iguazu, Misiones, Argentina, pp. 505-516.

Davies C. H., and X. Wang, 2001. Planimetric accuracy of IKONOS 1-m panchromatic image products, *Proceedings of the 2001 ASPRS Annual Conference*, 23 – 27 April, St. Louis, Missouri, (ASPRS, Bethesda, Maryland), unpaginated CD-ROM.

Fritz, L. W., 1996. The era of commercial earth observation satellites, *Photogrammetric Engineering & Remote Sensing*, 62(1):39-45.

Kaufmann, V., und W. Sulzer, 1997. Über die Nutzungsmöglichkeit hochauflösender amerikanischer Spionage-Satellitenbilder (1960-1972), *Vermessung und Geoinformation*, 3:166-173.

Konecny G., 2000. Mapping from space, *Remote Sensing for Environmental Data in Albania: A Strategy for Integrated Management*, 06-10 October, Tirana, Albania, (NATO Science Series, Vol. 72, Kluwer Academic Publishers, Dordrecht, The Netherlands), pp. 41-58.

Li, R., 1998. Potential of high-resolution satellite imagery for national mapping products, *Photogrammetric Engineering & Remote Sensing*, 64(12):1165-1170.

Meinel, G., M. Neubert and J. Reder, 2001. Pixelorientierte versus segmentorientierte Klassification von IKONOS-Satellitenbildendaten – ein Methodenvergleich. *Photogrammetrie Fernerkundung Geoinformation*, 3:157-170.

Ridley, H. M., P. M. Atkinson, P. Aplin, J.-P. Muller and I. Dowman 1997. Evaluating the potential of the forthcoming commercial U.S. high-resolution satellite sensor imagery at the Ordnance Survey®, *Photogrammetric Engineering & Remote Sensing*, 63(8):997-1005.

Toutin, Th., 1983. *Analyse mathématique des capacités stéréoscopiques du satellite SPOT*, Mémoire de DEA, Ecole Nationale des Sciences Géodésiques, Paris, France, 74 p.

Toutin, Th., 1995. Multisource data fusion with an integrated and unified geometric modelelling, *EARSeL Advances in Remote Sensing*, 4(2):118-129 (also available at http://www.ccrs.nrcan.gc.ca/ccrs/rd/sci_pub/bibpdf/1223.pdf).

Toutin, Th., and P. Cheng, 2000. Demystification of IKONOS, *Earth Observation Magazine*, 9(7):17-21 (also available at http://www.ccrs.nrcan.gc.ca/ccrs/rd/sci_pub/bibpdf/4807.pdf).

Zhou, G., and R. Li, 2000. Accuracy evaluation of ground points from IKONOS high-resolution satellite imagery, *Photogrammetric Engineering & Remote Sensing*, 66(9):1103-1112.